Mass Spectrometry
DOI: 10.5702/massspectrometry.A0132
Vol. 12 (2023), A0132

Original Article

Using Mass Spectrometry Imaging to Visualize Pesticide Accumulation and Time-Dependent Distribution in Fungicide-Coated Seeds

Shuichi Shimma[*,1,2,3], Hiromi Saito[1], Takuya Inoue[4], and Fukumatsu Iwahashi[4]

[1]*Department of Biotechnology, Graduate School of Engineering, Osaka University, Suita, Osaka 565–0871, Japan*
[2]*Osaka University Shimadzu Analytical Innovation Laboratory, Osaka University, Suita, Osaka 565–0871, Japan*
[3]*Institute for Open and Transdisciplinary Research Initiatives, Osaka University, 2–1 Yamadaoka, Suita, Osaka 565–0871, Japan*
[4]*Health & Crop Sciences Research Laboratory, Sumitomo Chemical Company, Ltd., 4–2–1 Takarazuka, Hyogo 665–8555, Japan*

Pesticide seed treatment provides efficient crop protection in the early season and enables a reduction in the quantity of fungicides used later. Hence, it has been a practical application for crop protection in major crop sectors such as corn, soybean, wheat, and cotton. The chemicals on pesticide-treated seeds may show different distributions depending on the structure of the seeds and the physical properties of the chemicals, but they have not been well studied because of a lack of versatile analytical tools. Here, we used mass spectrometry imaging to visualize the distribution of a fungicide (ethaboxam) in corn and soybean seeds coated with it. Contrasting distribution patterns were noted, which are likely dependent on the seed structure. We also obtained information on fungicide distribution after the seedings, which will contribute to a better understanding of the fungicide delivery pathway within plants. Using this new analytical method, we were able to obtain hitherto unavailable time-dependent, dynamic information on the ethaboxam. We expect that this method will be a useful tool with widespread applications in pesticide development and use.

Please cite this article as: Mass Spectrom (Tokyo) 2023; 12(1): A0132

Keywords: mass spectrometry imaging, fungicide, ethaboxam, pre- and post-seeding, fungicide-coated seeds

(Received February 24, 2023; Accepted September 15, 2023; advance publication released online September 28, 2023)

INTRODUCTION

Matrix-assisted laser desorption/ionization mass spectrometry imaging (MALDI-MSI) has been utilized in various fields as a non-labeling imaging method. To date, most studies utilizing MALDI-MSI have been conducted in medicine and pharmacology.[1,2] In recent years, however, this technique has also been applied to other areas of research, such as botany and microbiology, for the visualization of secondary metabolite distribution[3–7] and in the dynamic evaluation of pesticides.[8–13] The utility of this technique has attracted considerable interest regarding the visualization of pesticide distribution, which has hitherto relied on the somewhat restrictive use of ^{14}C-labeled pesticides and autoradiographic detection, as well as the time-dependent dynamic movements of pesticides within plants, for which there is currently limited information.[14,15]

Since the first systemic fungicide for seed treatment was introduced in the United States in the 1970s, pesticide seed treatments, such as seed coating, film coating, and pellet treatments, have provided efficient crop protection in the early season and have enabled a reduction in the quantity of pesticides applied to crops. This seed treatment technology has been a practical application for crop protection in major crop sectors, such as corn, soybean, wheat, and cotton.[16–18] Seed treatment applications with pesticides have been well established and optimized for each crop area. Pesticides applied to seeds are ultimately translocated to target plant tissues, either by direct migration or by transient translocation to the soil, followed by reabsorption.[19] However, there is currently limited information on the mechanisms by which the pesticides used for seed treatment are translocated in plant tissues. Such information could lead to a better understanding of the actual chemical distribution in plants and would contribute to the generation of novel applications for crop protection.

In this study, based on MALDI-MSI analyses, we sought to gain insights into the distribution of pesticides used for seed treatment. To this end, we coated the dried seeds of corn and soybean with the fungicide ethaboxam,[20–23] which is

*Correspondence to: Shuichi Shimma, *Institute for Open and Transdisciplinary Research Initiatives, Osaka University, 2–1 Yamadaoka, Suita, Osaka 565–0871, Japan,* e-mail: sshimma@bio.eng.osaka-u.ac.jp

particularly effective against oomycetes, and is used in spray and seed treatment applications, and visualized its distribution within the seeds both before and after germination. In this regard, it is difficult to prepare sections for imaging when using dry seeds as samples for MALDI-MSI, owing to seed hardness. Therefore, in the present study, we attempted to use a cryotape to prepare these sections.

Here we considered the use of a matrix and a method of sectioning. By using the method, we demonstrated that MALDI-MSI is a useful tool for evaluating the distribution of seed treatment applications.

MATERIALS AND METHODS

Chemicals

α-Cyano-4-hydroxycinnamic acid (α-CHCA) and 9-aminoacridine (9-AA) were purchased from Merck (MD, USA) and Tokyo Chemical Industry (Tokyo, Japan), respectively. Methanol, acetonitrile, formic acid, 2-propanol, and ultrapure water were purchased from Fujifilm Wako Pure Chemical Industries (Osaka, Japan). All reagents were of LC-MS grade.

Soybean and corn seed treatment with ethaboxam

Ethaboxam 34.2% (w/v) suspension concentrate (SC) formulation (INTEGO Solo fungicide; Nufarm, Calgary, Canada) was diluted with water to prepare the test solutions for seed treatment. Soybean (Variety: Hatayutaka) seeds were treated with the recommended concentration for an eventual ethaboxam dosage of 75.0 g a.i. (active ingredient)/100 kg seed. For seed treatments, soybean seeds (50 g) were placed in a 0.5-L plastic bag containing 260 µL of the test solution and shaken vigorously to coat the seeds. For corn (Variety: P1547) seeds, an eventual ethaboxam dosage of 37.5 g a.i./100 kg seed was applied by placing corn seeds (50 g) in a 0.5-L plastic bag containing 490 µL of test solution and shaking them vigorously.

Seed germination

Plastic cups (with a capacity of 0.75 oz) with holes in the bottom were filled with soil to approximately 80% capacity, and the coated soybean or corn seeds were planted at a depth of approximately 1 cm from the soil surface. After seeding, the cups were placed in a vat containing water at a depth of approximately 2 cm and incubated in a 25°C room.

Tissue preparation

For pre- and post-seeding seeds, we sectioned the seeds at −20°C using a cryomicrotome (CM1950; Leica, Nussloch, Germany) after flash freezing in liquid nitrogen. Cryosectioning was performed with the embedding of 4% carboxymethyl cellulose (SECTION-LAB, Yokohama, Japan). To collect sections, we used cryofilms (SECTION-LAB). All frozen tissues were sectioned at 15 µm. Sections on the cryofilm were mounted onto indium–tin–oxide (ITO)-coated glass slides (100 Ω/m^2 without anti-peeling coating; Matsunami Glass, Osaka, Japan) using a double-sided conductive tape (Shielding Non-woven Fabric Tape; 3M Company, MN, USA).

Matrix application

For the analysis of the standard material (control), we used α-CHCA solution in the positive ion detection mode at a concentration of 10 mg/mL. The solvent used was a mixture of acetonitrile, isopropanol, and water at a ratio of 60 : 10 : 30, and contained 0.1% formic acid. Additionally, the 9-AA solution in the negative ion detection mode was formulated using 70% methanol at a concentration of 5 mg/mL. When performing MALDI-MSI, the vacuum deposition equipment (iMLayer; Shimadzu, Kyoto, Japan) was coated with 0.7 µm of α-CHCA *via* vacuum deposition at approximately 1×10^{-2} Pa.

Mass spectrometry (MS) of the standard sample and mass spectrometry imaging of seeds sections

MS of the standard sample and MALDI-MSI on sample surfaces were performed using a new quadrupole-time-of-flight-type mass microscope (iMScope QT; Shimadzu).[24] iMScope QT has an atmospheric-pressure sample chamber for observation and an Nd : YAG laser (λ = 355 nm and 1 kHz) as the atmospheric-pressure MALDI ionization source. Therefore, it was possible to obtain optical images and determine the ion distribution within a microscopic view of the same instrument. Laser irradiation was performed on the tissue surface with 50 shots at each data point. In MSI, the pixel size was 50 × 50 µm. Mass spectra were acquired in both positive and negative ion detection modes in the mass ranges of *m/z* 300–330 for mass spectra and *m/z* 100–330 for product ion spectra. In MALDI-MSI experiments using iMScope QT, a constant voltage of the detector was applied (2.1 kV in single MS analysis and 2.3 kV in MS/MS analysis). The laser diameter (*d*) and power (*LP*) were maintained at a constant value of $d = 2$ and $LP = 65$ (arbitrary units in the iMScope QT). To obtain an ethaboxam signal, MS/MS analysis was performed using a selected precursor ion of *m/z* 321 in the positive ion detection mode and *m/z* 319 in the negative ion detection mode.

Image reconstruction and data analysis

Ion image reconstruction and data analyses were performed using IMAGEREVEAL MS (Shimadzu). All images were displayed at absolute intensity. In addition, linear interpolation was performed for all images.

RESULTS

Verification of ethaboxam ionization

Figure 1 shows the mass and product ion spectra obtained in the positive ion detection mode using α-CHCA and in the negative ion detection mode using 9-AA. Figure 1A shows the chemical structure of ethaboxam and the expected *m/z* for each polarity. The peak at *m/z* 321.08 was from the protonated ion in the positive ion detection, while the peak at *m/z* 319.07 was from the deprotonated ion in the negative ion detection. Figure 1B shows that *m/z* 321.08 was detected when α-CHCA was used as a matrix to obtain the mass spectrum, whereas *m/z* 319.06 was not detected when 9-AA was used (Fig. 1C). Subsequently, we confirmed whether the product ions were detected. As a result, the product ions were detected at *m/z* 183.05, 200.07, and 237.08 with α-CHCA (Fig. 1B), and no peaks could be obtained when 9-AA was used. Despite attempting to perform negative ion detection using 9-AA, even with the high-concentrate standard sample, the peaks of the ion were not detected. Therefore, we decided to use the positive ion detection mode using α-CHCA. In addition, we decided to use the peak at *m/z* 321.08 or the product ion at *m/z* 183.05 for visualization.

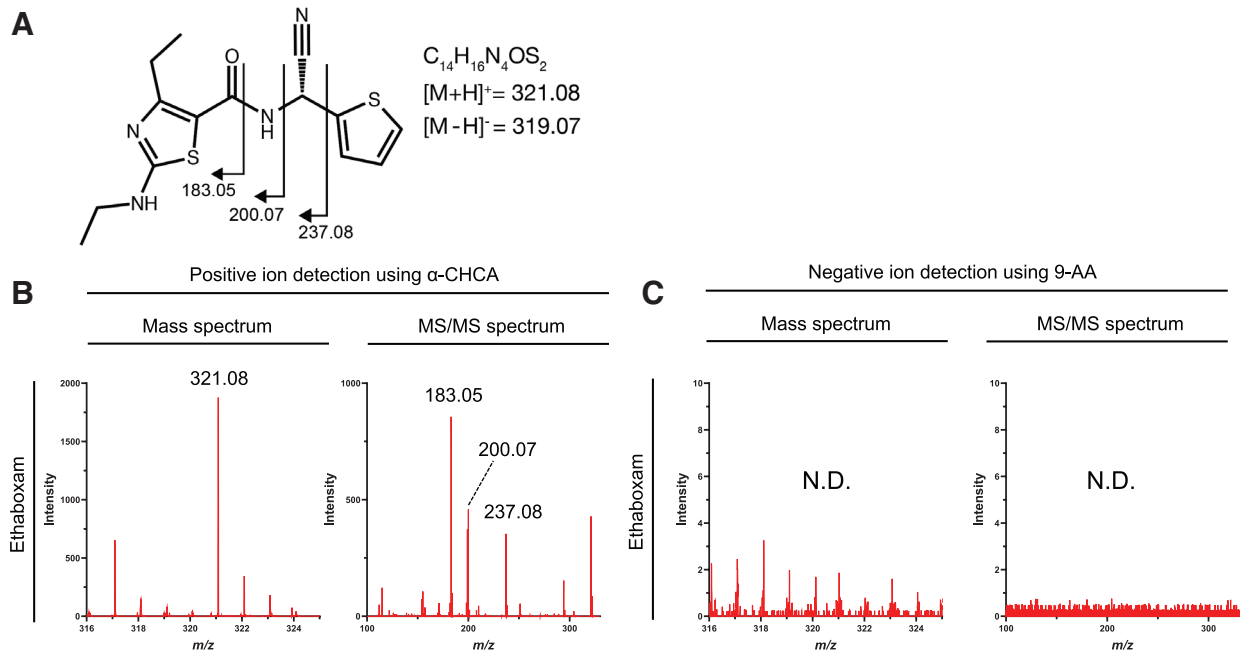

Fig. 1. Verification of ethaboxam ionization using MALDI. (A) The ethaboxam structural and composition formulae. (B) Mass and product ion spectra of ethaboxam obtained using the positive ion detection mode. (C) Mass and product ion spectra of ethaboxam obtained using the negative ion detection mode. With the negative ion detection mode, a peak was obtained at *m/z* 319.06, but compared with the positive ion detection mode, the intensity was extremely low. In contrast, with the positive ion mode, a peak was obtained at *m/z* 321.0, and this indicated that a peak derived from the structure could also be obtained in the product ion spectrum. α-CHCA, α-cyano-4-hydroxycinnamic acid; MALDI, matrix-assisted laser desorption; MS, mass spectrometry; ND, not detected.

Ethaboxam distribution in pre-seeding seed sample (Day 0)

In performing MALDI-MSI with α-CHCA, we used iMLayer, an automated matrix deposition device. Using this device, we deposited a 0.7-μm thick matrix layer. The results of these measurements are shown in Fig. 2. Ethaboxam was visualized in soybean seeds and corn seeds by detection of *m/z* 321.084. Under the condition, ethaboxam was accumulated on the surface of both seeds at a high intensity (Fig. 2A and 2B). In the soybean seed, the peak intensity was homogeneous on the surface. On the other hand, the high-intensity region was found on the tip of the seed and inside the seed (Fig. 2B, arrowheads). In addition, we can confirm that there was no distribution without ethaboxam treatment.

The obtained mass spectra are shown in Fig. S1. Here, we confirmed a low background peak at *m/z* 321.087, which was 0.03 higher *m/z* value, in the untreated corn sample. The mass resolution of iMScope QT was 25,000 for the ethaboxam peak in single MS. This mass resolution could not separate between the peaks of *m/z* 321.084 and *m/z* 321.087. Therefore, we performed MS/MS for visualization. The results are shown in Fig. S2. By using product ion peaks for visualization, the background signal was completely removed. For both soybean seeds and corn seeds, the distribution was not changed; however, we considered the specificity became improved (Fig. 3A and 3B). In the following experiment, we performed MS/MS imaging to visualize ethaboxam distribution.

Germinated soybean and corn seeds imaging results (Day 1)

After the soybean and corn seeds had been planted in the soil, the seeds were sampled on the first day after seeding to visualize the distribution of ethaboxam. Given that an ethaboxam-derived peak was obtained on the surface of soybean and corn seeds, we expected to observe ethaboxam-derived signals post-seeding. In line with this expectation, we were able to detect high-intensity ethaboxam signals on the surface of seeds (Fig. 4A and 4B). Especially, we confirmed the ethaboxam signal even inside the seeds (arrowheads around the embryo in Fig. 4B). These findings indicate that ethaboxam migrates over time after seeding. On the other hand, we were not able to detect signal peaks from the negative control samples (Fig. S3).

Germinated soybean seeds and corn seeds imaging results (Day 5)

Soybean seeds and corn seeds were sampled on the fifth day after seeding, and ethaboxam distribution was visualized (Fig. 5). We found that the ethaboxam signal intensity was considerably lower than that Day 1 in soybean (Fig. 5A). On the other hand, in corn seeds, the ethaboxam remained on the seed surface. In addition, the signal intensity inside the seeds (around the embryo) was increased (Fig. 5B, arrowheads). The signal was also above the noise level (Fig. S4). Based on these observations, we assumed that even after ethaboxam has accumulated on the seed coat at the seed stage of the plant, it was likely that the pesticide migrates from the seed coat to the cotyledon after seeding.

DISCUSSION

Given that ethaboxam has a high nitrogen content (Fig. 1A), positive ion detection was considered superior to negative ion detection. In the positive ion detection, the peak at *m/z* 321.08 was set as the precursor ion. In the obtained

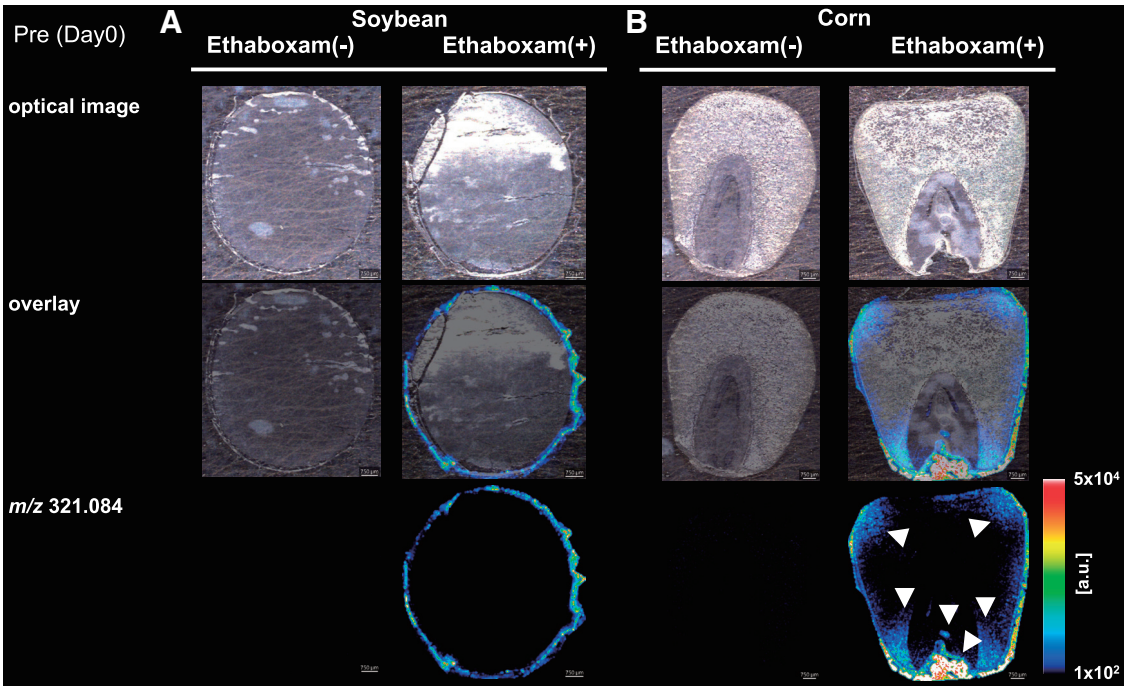

Fig. 2. Ethaboxam distribution in soybean seeds and corn seeds using single MS (*m/z* 321.084). (A) Optical image of the soybean seed section, overlay image, and ethaboxam image with and without ethaboxam treatment. (B) Optical image of the corn seed section, overlay image, and ethaboxam image with and without ethaboxam treatment. Arrowheads indicate ethaboxam accumulated regions. Scale bars: 750 μm. MS, mass spectrometry.

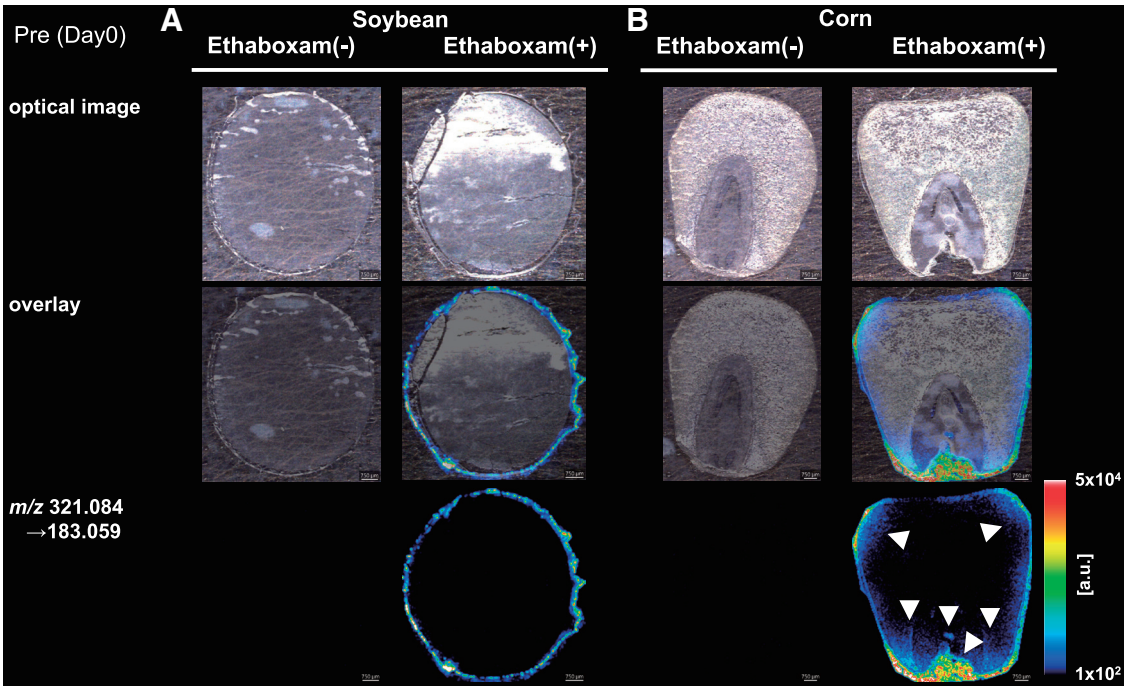

Fig. 3. Ethaboxam distribution in soybean seeds and corn seeds using product ion MS (*m/z* 321.084 >183.059). (A) Optical image of the soybean seed section, overlay image, and ethaboxam image with and without ethaboxam treatment. (B) Optical image of the corn seed section, overlay image, and ethaboxam image with and without ethaboxam treatment. Arrowheads indicate ethaboxam accumulated regions. Scale bars: 750 μm. MS, mass spectrometry.

product ion spectrum, the peaks of *m/z* 183.05, 200.07, and 237.08 were clearly detected. We performed the interpretation of the obtained product ion spectrum using the mass shift law.[25] Based on the law, the cleavages were confirmed at the site indicated in Fig. 1A. Therefore, it was decided to perform product ion MS in the positive ion detection mode on the sample surface and monitor the intensity of the peak at *m/z* 183.05 (the base peak of the product ion spectrum) to obtain information on the spatial distribution of ethaboxam.

Previously, the use of MSI to analyze seed material has been reported based on time-of-flight secondary ion mass

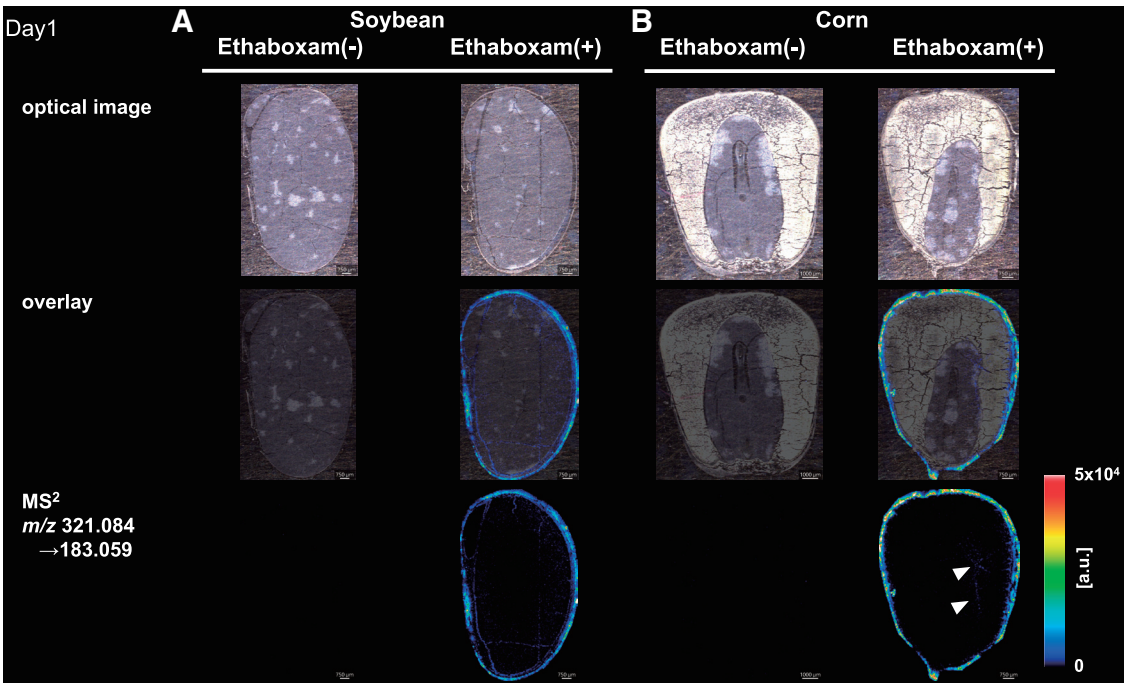

Fig. 4. Ethaboxam distribution in post-seeding soybean seeds and corn seeds in Day 1. (A) Optical image of the soybean seed section, overlay image, and ethaboxam image with and without ethaboxam treatment. (B) Optical image of the corn seed section, overlay image, and ethaboxam image with and without ethaboxam treatment. Arrowheads indicate ethaboxam accumulated region around the embryo in the corn seed section. Scale bars: soybean seed 750 μm, corn seed without ethaboxam treatment 750 μm, and corn seed with ethaboxam treatment 1000 μm. MS, mass spectrometry.

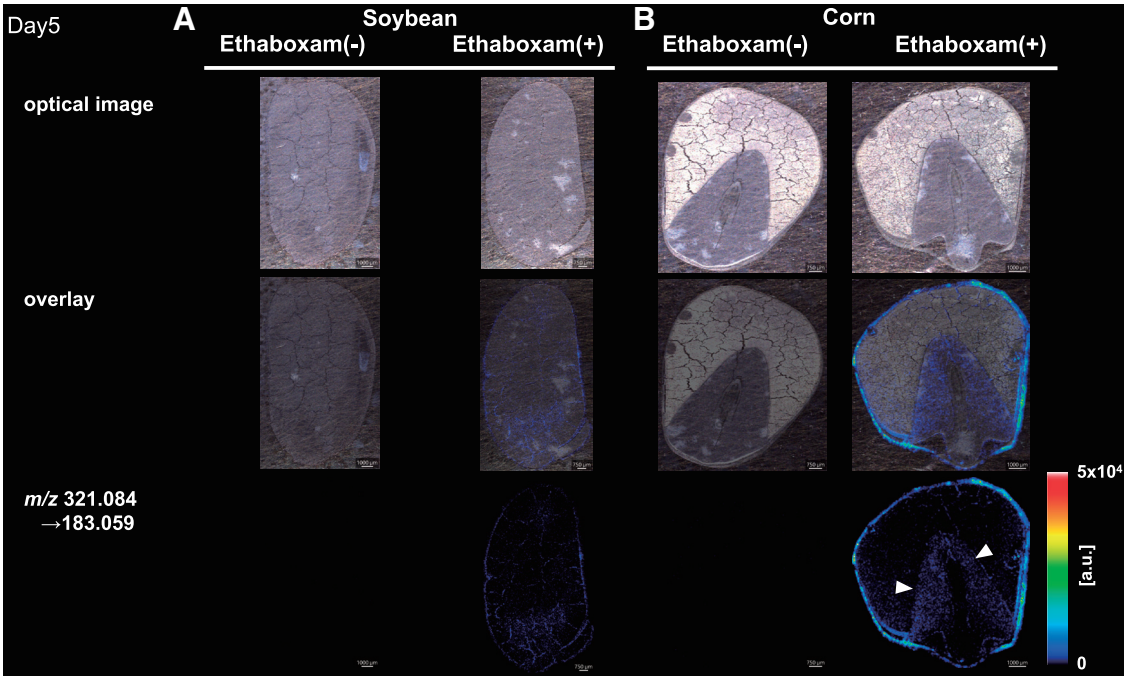

Fig. 5. Ethaboxam distribution in post-seeding soybean seeds and corn seeds in Day 5. (A) Optical image of the soybean seed section, overlay image, and ethaboxam image with and without ethaboxam treatment. (B) Optical image of the corn seed section, overlay image, and ethaboxam image with and without ethaboxam treatment. Arrowheads indicate ethaboxam accumulated region around the embryo in the corn seed section. Scale bars: treated soybean seeds and untreated corn seeds 750 μm, and untreated soybean and treated corn seed 1000 μm.

spectrometry measurements.[26] In the previous study, the authors described the pre-processing of raw corn seed samples, in which better sectioning was achieved using an adhesive tape. In our study, the adhesive tape (Cryofilm) maintained excellent morphology of the samples. Sections with very good morphology could also be produced in germinated soybean seeds and germinated corn seeds with a high water content.

Figure 2 shows the distribution of ethaboxam in the different sections of the seeds prior to germination. A comparison of the peak intensity in the different regions in Figs. S5 and

S6 indicates that for soybean and corn seeds, the ethaboxam intensity was relatively high on the seed surface. This result suggested that the ethaboxam tended to accumulate on the seed surface.

With germinated ethaboxam-coated corn seeds, signals were obtained from within the seed, and ethaboxam accumulation was also observed around the radicle or root (Fig. 5B, arrowheads). In the case of soybean seeds, the intensity of the ions was strongest on the seed coat, and the levels decreased from the surface of the seed coat toward the seed interior. In addition, the peak intensity was dramatically decreased on the Day 5 (Fig. S5). These observations suggest that in soybean seeds coated with ethaboxam, the pesticide remained mainly on the surface of the seed coat and is released into the soil over time. The observed differences in the distribution of ethaboxam after seeding are assumed to be related to differences in the seed structure, particularly with regard to the presence of an endosperm. In a corn seed, an endosperm seed, we detected ethaboxam accumulation in the embryo after coating the seed with the chemical (Fig. 2B). Therefore, if the distribution of pesticides is very different at the stage prior to seeding, we might expect that pesticide migration would also be significantly affected by this difference. Intensity graphs of ethaboxam on the surface and in the embryo of post-seeding corn seeds depict a marked change in the distribution pattern from Day 1 to Day 5 (Fig. S6), with a pronounced shift from the embryo to the endosperm. We concluded that the ethaboxam coated onto the seed had started to migrate into and within the seed.

In contrast, in the case of soybean seeds, on the Day 1 post-seeding, ethaboxam was detected on the seed surface, whereas the quantity detected within the seed was low (Fig. S5 inside). This tendency became more apparent on the Day 5 after seeding (Fig. S5 inside), indicating that there was very little or no direct migration of ethaboxam from the seed coat to the internal parts of the seed.

Based on the findings of this study, we demonstrated that MALDI-MSI is a useful technique for visualizing the distribution of seed-coated pesticides before and after seeding. Notably, we found that the same pesticide showed different patterns of distribution that were dependent on the seed structure. In the case of soybean seeds, we observed that ethaboxam accumulated predominantly on the seed coat, and almost no direct migration of the pesticide to the seed interior was detected after germination. In contrast, the direct migration of ethaboxam into the plant tissue was more pronounced in the corn than in the soybean, indicating a different balance of dependent transfer pathways.

Seed treatment agents are transferred to plant tissues for protection from phytopathogens by direct transfer to the plant or indirect transfer through the soil. By visualizing the localization of the compound together with the partial structure of the seed, we propose that the ratio involved in the migration of the compound differs depending on the seed type and structure. Such behavior of seed-treated compounds would depend on the physical properties of each chemical and species-specific seed structure. Therefore, MSI is expected to facilitate the development of seed treatment applications, such as optimization of formulations, by understanding pesticide distributions in the target seeds.

ACKNOWLEDGMENTS

The authors are grateful to Prof. Junko Iida at Osaka University Shimadzu Analytical Innovation Laboratory for permitting the use of the iMScope QT, iMLayer, and other instruments for this research.

CONFLICTS OF INTEREST

The authors declare no conflicts of interest.

REFERENCES

1) S. Shimma, H. O. Kumada, H. Taniguchi, A. Konno, I. Yao, K. Furuta, T. Matsuda, S. Ito. Microscopic visualization of testosterone in mouse testis by use of imaging mass spectrometry. *Anal. Bioanal. Chem*. 408: 7607–7615, 2016.
2) Y. Sugiura, E. Takeo, S. Shimma, M. Yokota, T. Higashi, T. Seki, Y. Mizuno, M. Oya, T. Kosaka, M. Omura, T. Nishikawa, M. Suematsu, K. Nishimoto. Aldosterone and 18-oxocortisol coaccumulation in aldosterone-producing lesions. *Hypertension* 72: 1345–1354, 2018.
3) D. S. Dalisay, K. W. Kim, C. Lee, H. Yang, O. Rubel, B. P. Bowen, L. B. Davin, N. G. Lewis. Dirigent protein-mediated lignan and cyanogenic glucoside formation in flax seed: Integrated omics and MALDI mass spectrometry imaging. *J. Nat. Prod*. 78: 1231–1242, 2015.
4) A. C. Crecelius, D. Holscher, T. Hoffmann, B. Schneider, T. C. Fischer, M. V. Hanke, H. Flachowsky, W. Schwab, U. S. Schubert. Spatial and temporal localization of flavonoid metabolites in strawberry fruit (*Fragaria x ananassa*). *J. Agric. Food Chem*. 65: 3559–3568, 2017.
5) T. B. Nguyen, S. Kitani, S. Shimma, T. Nihira. Butenolides from *Streptomyces albus* J1074 Act as external signals to stimulate avermectin production in *Streptomyces avermitilis*. *Appl. Environ. Microbiol*. 84: e02791–17, 2018.
6) K. Miyoshi, Y. Enomoto, E. Fukusaki, S. Shimma. Visualization of asparaptine in asparagus (*Asparagus officinalis*) using MALDI-IMS. *Anal. Sci*. 34: 997–1001, 2018.
7) S. J. B. Dunham, J. F. Ellis, B. Li, J. V. Sweedler. Mass spectrometry imaging of complex microbial communities. *Acc. Chem. Res*. 50: 96–104, 2017.
8) D. M. Anderson, V. A. Carolan, S. Crosland, K. R. Sharples, M. R. Clench. Examination of the distribution of nicosulfuron in sunflower plants by matrix-assisted laser desorption/ionisation mass spectrometry imaging. *Rapid Commun. Mass Spectrom*. 23: 1321–1327, 2009.
9) D. M. Anderson, V. A. Carolan, S. Crosland, K. R. Sharples, M. R. Clench. Examination of the translocation of sulfonylurea herbicides in sunflower plants by matrix-assisted laser desorption/ionisation mass spectrometry imaging. *Rapid Commun. Mass Spectrom*. 24: 3309–3319, 2010.
10) S. P. Annangudi, K. Myung, C. Avila Adame, J. R. Gilbert. MALDI-MS imaging analysis of fungicide residue distributions on wheat leaf surfaces. *Environ. Sci. Technol*. 49: 5579–5583, 2015.
11) C. Bedia, R. Tauler, J. Jaumot. Analysis of multiple mass spectrometry images from different *Phaseolus vulgaris* samples by multivariate curve resolution. *Talanta* 175: 557–565, 2017.
12) S. Gerbig, H. E. Brunn, B. Spengler, S. Schulz. Spatially resolved investigation of systemic and contact pesticides in plant material by desorption electrospray ionization mass spectrometry imaging (DESI-MSI). *Anal. Bioanal. Chem*. 407: 7379–7389, 2015.
13) A. K. Mullen, M. R. Clench, S. Crosland, K. R. Sharples. Determination of agrochemical compounds in soya plants by imaging matrix-assisted laser desorption/ionisation mass spectrometry. *Rapid Commun. Mass Spectrom*. 19: 2507–2516, 2005.
14) F. Fadel Sartori, R. Floriano Pimpinato, V. L. Tornisielo, T. Dieminger Engroff, D. de Souza Jaccoud-Filho, J. O. Menten, A. E.

Dorrance, D. Dourado-Neto. Soybean seed treatment: How do fungicides translocate in plants? *Pest Manag. Sci*. 76: 2355–2359, 2020.
15) M. Kubicki, M. Lamshoft, A. Lagojda, M. Spiteller. Metabolism and spatial distribution of metalaxyl in tomato plants grown under hydroponic conditions. *Chemosphere* 218: 36–41, 2019.
16) K. K. Sharma, U. S. Singh, P. Sharma, A. Kumar, L. Sharma. Seed treatments for sustainable agriculture—A review. *J. Appl. Nat. Sci*. 7: 521–539, 2015.
17) A. E. Dorrance, S. A. McClure. Beneficial effects of fungicide seed treatments for soybean cultivars with partial resistance to *Phytophthora sojae*. *Plant Dis*. 85: 1063–1068, 2001.
18) M. L. Ellis, K. D. Broders, P. A. Paul, A. E. Dorrance. Infection of soybean seed by *Fusarium graminearum* and effect of seed treatments on disease under controlled conditions. *Plant Dis*. 95: 401–407, 2011.
19) A. Alford, C. H. Krupke. Translocation of the neonicotinoid seed treatment clothianidin in maize. *PLoS One* 12: e0186527, 2017.
20) D. S. Kim, S. J. Chun, J. J. Jeon, S. W. Lee, G. H. Joe. Synthesis and fungicidal activity of ethaboxam against Oomycetes. *Pest Manag. Sci*. 60: 1007–1012, 2004.
21) W. Hao, M. A. Gray, H. Förster, J. E. Adaskaveg. Evaluation of new Oomycota fungicides for management of *Phytophthora* root rot of citrus in California. *Plant Dis*. 103: 619–628, 2019.
22) K. Scott, M. Eyre, D. McDuffee, A. E. Dorrance. The efficacy of ethaboxam as a soybean seed treatment toward *Phytophthora*, *Phytopythium*, and *Pythium* in Ohio. *Plant Dis*. 104: 1421–1432, 2020.
23) M. Wang, S. Van Vleet, R. McGee, T. Paulitz, L. Porter, K. Schroeder, G. Vandemark, W. Chen. Chickpea seed rot and damping-off caused by Metalaxyl-resistant *Pythium ultimum* and its management with ethaboxam. *Plant Dis*. 105: 1728–1737, 2021.
24) S. Ikuta, N. Shinohara, E. Fukusaki, S. Shimma. Mass spectrometry imaging enables visualization of the localization of glutamate decarboxylase activity in germinating legume seeds. *J. Biosci. Bioeng*. 134: 356–361, 2022.
25) H. Nakata. A rule to account for mass shifts of even-electron fragment ions in fast-atom bombardment mass spectrometry. *Eur. J. Mass Spectrom*. 5: 411–418, 1999.
26) S. H. Kim, J. Kim, Y. J. Lee, T. G. Lee, S. Yoon. Sample preparation of corn seed tissue to prevent analyte relocations for mass spectrometry imaging. *J. Am. Soc. Mass Spectrom*. 28: 1729–1732, 2017.